Imaging Conductivity using Electric Properties Tomography – Initial Clinical Results in Glioma Patients

Tobias Voigt[1]

[1]Philips Research, 4th floor Lambeth Wing, St Thomas Hospital, London, United Kingdom,
tobias.voigt@philips.com

Abstract

The electric properties of human tissue can potentially be used as an additional diagnostic parameter, e.g., in tumour diagnosis. In the framework of radiofrequency (RF) safety, the electric conductivity of tissue is needed to correctly estimate the local specific absorption rate (SAR) distribution during magnetic resonance imaging (MRI). In this study, a recently developed approach, called electric properties tomography (EPT) is applied to *in vivo* imaging in a clinical setting. It derives the patient's electric conductivity and permittivity from the spatial sensitivity distributions of the RF coils in MRI. In contrast to other methods to measure the patient's electric properties, EPT does not apply externally mounted electrodes, currents, or RF probes, which enhances the practicability of the approach.
This work shows that conductivity distributions can be reconstructed from phase images of the RF transmit field. Using this approximation, three-dimensional *in vivo* conductivity maps of the human brain are obtained in 6 min. We report first practical experiences of conductivity imaging in patients with brain glioma in a real-world clinical environment. *In vivo* conductivity of glioma is measured for two patients and quantitative values are compared with white matter conductivities of healthy volunteers. Glioma conductivity was found to be significantly higher than healthy white matter conductivity.

1. Introduction

MRI provides a vast variety of possible image contrasts. Contrasts comprising quantitative parameters are of particular clinical interest due to reasons of reproducibility and comparability. Electric conductivity and permittivity are possible candidates for quantitative parameters. The idea of extracting electric properties from MR images was already proposed in 1991 (1). Only recently, the electric properties of the human body have been applied as a quantitative image contrast in standard MRI via electric properties tomography (EPT) (2). EPT allows the determination of the conductivity and permittivity using the radiofrequency (RF) transmit field map of a standard MR scan.

The task of imaging electric properties has been addressed by a variety of imaging modalities. All these methods differ from the EPT approach, which uses a standard MR system and requires neither electrode mounting nor the application of additional RF energy. Instead, the EPT approach employs post-processing the field map of the imaging RF pulse. Since electrical properties are in general frequency dependent, EPT yields quantitative values for conductivity and permittivity at MR Larmor Frequency.

Knowledge of electric properties is not only of potential diagnostic value (3-5), but also crucial in the field of RF safety. The local heating of tissue is a major problem at high field MR, particularly in the framework of parallel transmission. The acceptable local specific absorption rate (SAR), which is directly related to tissue heating, may limit the parameter space available for the application of specific MR sequences. An exact determination of local SAR has to be based on patient specific dielectric properties of tissue. The EPT approach provides a step towards patient specific local SAR determination.

In this work, phase-based conductivity imaging is tested in simulation studies. Phase-based conductivity imaging is applied to healthy volunteers and white matter conductivity is compared to glioma conductivity measured in two patients.

978-1-4244-6051-9/11/$26.00

2. Theory

EPT relates the patient's electric properties to quantities that are accessible via MRI. The transmitted RF pulse is affected by the conductivity σ and permittivity ε of the tissue being imaged. In EPT formalism, the magnetic field strength vector **H** and the electric field vector **E**, corresponding to the RF fields of the MR system, are assumed to be time-harmonic **H, E** ~ exp($i\omega t$). Fields in MRI are best described using circularly polarized coordinates. In these coordinates, the magnetic field vector reads $\mathbf{H} = (H_p,\ H_m,\ H_z)^{\mathrm{T}}$ with $H_p = \frac{1}{\sqrt{2}}\left(H_x + iH_y\right)$, $H_m = \frac{1}{\sqrt{2}}\left(H_x - iH_y\right)$ and the z-component $H_z = H_{z,cart}$. H_p couples to the proton spins, and thus, is accessible via MR. The EPT approach links the desired electric properties $\kappa = \varepsilon - i\sigma/\omega$ to this measurable component via (6)

$$-\frac{\oint_{\partial V} \nabla H_p(\mathbf{r}) \cdot \mathrm{d}\mathbf{a}}{\omega^2 \mu \int_V H_p(\mathbf{r}) \mathrm{d}V} \approx \kappa(\mathbf{r}) \qquad [1]$$

with ω being the Larmor frequency, the integration volume is denoted by V, its surface by ∂V, and the surface element by d**a**. Eq. 1 depends only on the measurable H_p, i.e., the positively rotating component of the transmit field, as it is the case in (1, 7-9).

To obtain separate equations for σ and ε, the differentiation in Eq. 1 is executed explicitly taking into account that $H_p = \mu^{-1} B_p \exp(i\varphi_p)$. Here, B_p represents the magnitude of the positively rotating component of the RF transmit field and φ_p its phase.

Using the first Green's identity in the numerator of Eq. 1 and separating real and complex parts yields the expressions

$$\sigma(\mathbf{r}) = (\omega\mu V)^{-1}\left(\oint_{\partial V} \nabla\varphi_p(\mathbf{r}) \cdot \mathrm{d}\mathbf{a} + 2\int_V \left[\nabla \ln\left(B_p(\mathbf{r})\right) \cdot \nabla\varphi_p(\mathbf{r})\right] \mathrm{d}V\right) \qquad [2]$$

$$\varepsilon(\mathbf{r}) = \left(\omega^2 \mu \int_V B_p(\mathbf{r}) \mathrm{d}V\right)^{-1}\left[\int_V \left(\nabla\varphi_p(\mathbf{r})\right)^2 B_p(\mathbf{r}) \mathrm{d}V - \oint_{\partial V} \nabla B_p(\mathbf{r}) \cdot \mathrm{d}\mathbf{a}\right] \qquad [3]$$

Equations 2 and 3 are stated for compartments with constant κ. Approximate expressions for σ and ε can be obtained from Eqs. 2 and 3 assuming that terms containing both B_p and φ_p are small. The conductivity can thereby be expressed as function of the phase only

$$\sigma \approx \frac{1}{\mu_0 \omega V} \oint_{\partial V} \nabla\varphi_p(\mathbf{r}) \cdot \mathrm{d}\mathbf{a} \qquad [4]$$

and the permittivity can be related to the magnitude only

$$\varepsilon \approx \frac{-\oint_{\partial V} \nabla B_p(\mathbf{r}) \cdot \mathrm{d}\mathbf{a}}{\mu_0 \omega^2 \int_V B_p(\mathbf{r}) \mathrm{d}V} \qquad [5]$$

Equations 4 and 5 are particularly favourable, since conductivity and permittivity imaging can be split into separate measurements. On the one hand, for conductivity imaging, only the transmit phase has to be determined, skipping the magnitude measurement. On the other hand, in the case of permittivity imaging, only the magnitude has to be determined, skipping an additional phase measurement.

Please note that Eqs. 2 and 3 as well as Eqs. 4 and 5 provide absolute values of κ. Any scaling factors of the magnetic field's magnitude cancel out by dividing. For the sake of a clearer scope, this work is focused on conductivity imaging.

3. Methods

To validate the approximations made in phase-based conductivity imaging, FDTD simulations using the visible human and a quadrature body coil model were conducted in SEMCAD (Schmid & Partner Engineering AG, Zürich, Switzerland). The software provided necessary field components for conductivity reconstruction. Conductivity was reconstructed twice, according to the exact Eq. 2 and using the approximation Eq. 4.

For the *in vivo* part of the study, two patients with brain glioma were investigated as well as 5 healthy volunteers. All scans were conducted on a 1.5T scanner (Philips Healthcare, Best, The Netherlands) in a clinical environment. For phase-based conductivity imaging, a 3D TSE scan was used for phase mapping (FOV 210 × 200 ×

189 mm³, resolution 1.8 × 1.8 mm² in plane, 5 mm slice thickness, TR / TE = 400 / 5.4 ms, turbo factor 3, total scan time 6:20 min). Conductivity reconstruction was performed according to the reconstruction formula Eq. 4. Average values for conductivity were computed inside manually delineated white matter and glioma regions of interest.

4. Results

Reconstruction results using simulation data are shown in Fig. 1. Reconstructing conductivity from phase images only has little impact on image quality. Reconstructed quantitative conductivity values differ from expected values by approx 5-10% (see Tab. 1).

Average conductivity values for white matter of healthy volunteers and patients with glioma are shown in Tab. 2. The average white matter conductivity was 0.36 ± 0.05 S/m in healthy volunteers. Glioma conductivity was significantly higher at 1 ± 0.04 S/m. Conductivity images of the two patients investigated are shown in Fig. 2.

It is expected that white matter tissue structure affected by glioma is significantly altered. Cell conductivity at MR Larmor frequency is determined by the composition of intracellular cytoplasm. Our findings of enhanced conductivity in glioma suggest an alteration of tissue composition, e.g. vasculature, and/or alteration the cell interior, e.g. salt, water, or protein content compared with healthy white matter tissue.

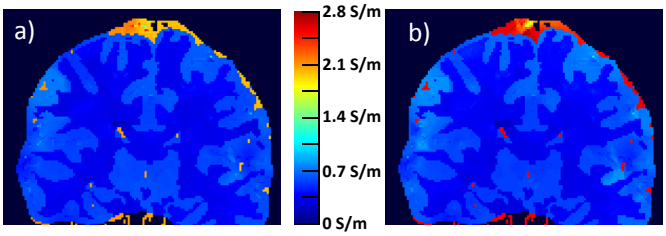

Figure 1: Reconstructed conductivity according to Eq. 1 (a) and using the phase-based approximation Eq. 2 (b).

ROI	Conductivity [S/m]	
	Exact formula	Phase based approximation
WM	0.30 ± 0.03	0.33 ± 0.04
GM	0.52 ± 0.06	0.57 ± 0.07
CSF	2.09 ± 0.12	2.19 ± 0.08

Table 1: Analysis of FDTD results shown in Fig. 1. Quantitative comparison of average values of conductivity inside different regions of interest.

Healthy volunteers	White matter ROI
1	0.43 ± 0.15
2	0.33 ± 0.11
3	0.37 ± 0.15
4	0.37 ± 0.23
5	0.3 ± 0.18

Patients	Glioma ROI
1	0.97 ± 0.18
2	1.02 ± 0.37

Table 2: Quantitative conductivity values of white matter in healthy volunteers and glioma in two patients. Corresponding images are shown in Fig. 2. ROIs have been drawn manually.

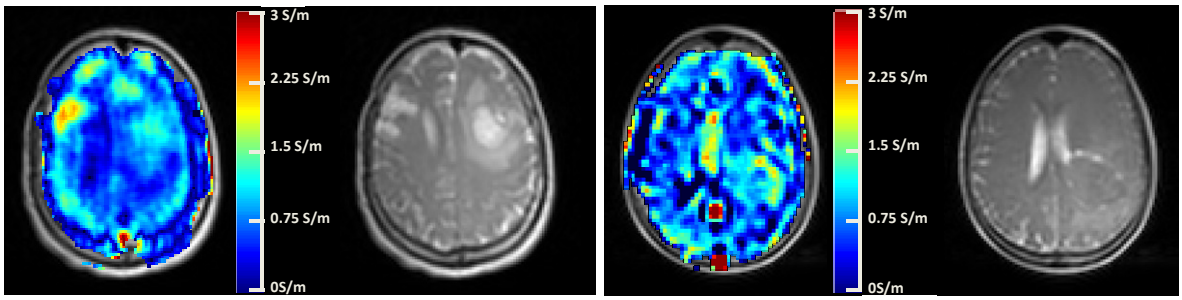

Figure 2: *In vivo* conductivity maps of glioma patients. Patient 1 (left) had a previous lesion excised on the opposite side. Patient 2 is shown on the right.

5. Conclusion

The presented approximations enable dedicated MR-EPT conductivity or permittivity imaging. Phase-based conductivity imaging yields highly accurate, high-resolution quantitative conductivity images within a clinically acceptable scan time.
Image acquisition protocols and post-processing have been established in a routine clinical environment. First clinical results are presented and *in vivo* conductivity of glioma is measured and compared with healthy white matter conductivity. First hints towards altered tissue composition and/or cellular constituents in glioma tissue are obtained via this new image contrast. In future work, the patient basis has to be extended and the cause of enhanced glioma conductivity has to be confirmed in histology.

6. Acknowledgments

The author thanks Ulrich Katscher, Christian Findeklee and Christian Stehning for significant contributions to EPT in general and the work presented in this article.

7. References

1. Haacke EM, Petropoulos LS, Nilges EW, Wu DH. Extraction of conductivity and permittivity using magnetic resonance imaging. *Phys Med Biol* 1991;38:723-734.

2. Katscher U, Voigt T, Findeklee C, Vernickel P, Nehrke K, Doessel O. Determination of Electric Conductivity and Local SAR via B1 Mapping. *IEEE Trans Med Imaging* 2009;28:1365-1374.

3. Schaefer M, Gross W, Ackemann J, Gebhard MM. The complex dielectric spectrum of heart tissue during ischemia. *Bioelectrochemistry* 2002;58:171-180.

4. Liu L, Dong W, Ji X, Chen L, Chen L, He W, Jia J. A new method of non-invasive brain-edema monitoring in stroke: cerebral electrical impedance measurement. *Neurol Res* 2006;28:31-37.

5. Joines WT, Zhang Y, Li C, Jirtle RL. The measured electrical properties of normal and malignant human tissues from 50 to 900 MHz. *Med Phys* 1994;21:547-550.

6. Voigt T, Katscher U, Doessel O. Quantitative Conductivity and Permittivity Imaging of the Human Brain using Electric Properties Tomography. *Magn Reson Med*, in press.

7. Cloos MA, Bonmassar G. Towards Direct B1 Based Local SAR Estimation. In *Proceedings of the 17th Annual Meeting of ISMRM*, Honolulu, Hawaii, USA 2009. p. 3037.

8. Bulumulla SB, Yeo TB, Zhu Y. Direct calculation of tissue electrical parameters from B1 maps. In *Proceedings of the 17th Annual Meeting of ISMRM*, Honolulu, Hawaii, USA 2009. p. 3043.

9. Wen H. Noninvasive quantitative mapping of conductivity and dielectric distributions using RF wave propagation effects in high-field MRI. In *Proceedings of SPIE* 2003;5030:471-477.